THE JOURNAL OF PHYSICAL CHEMISTRY Letters

pubs.acs.org/JPCL Letter

Water Structure, Dynamics, and Sum-Frequency Generation Spectra at Electrified Graphene Interfaces

Yiwei Zhang, Hilton B. de Aguiar, James T. Hynes, and Damien Laage*

Cite This: J. Phys. Chem. Lett. 2020, 11, 624−631 Read Online

ACCESS | Metrics & More | Article Recommendations | Supporting Information

ABSTRACT: The properties of water at an electrified graphene electrode are studied via classical molecular dynamics simulations with a constant potential approach. We show that the value of the applied electrode potential has dramatic effects on the structure and dynamics of interfacial water molecules. While a positive potential slows down the reorientational and translational dynamics of water, an increasing negative potential first accelerates the interfacial water dynamics before a deceleration at very large magnitude potential values. Further, our spectroscopic calculations indicate that the water rearrangements induced by electrified interfaces can be probed experimentally. In particular, the calculated water vibrational sum-frequency generation (SFG) spectra show that SFG specifically reports on the first two water layers at 0 V but that at larger magnitude applied potentials the resulting static field induces long-range contributions to the spectrum. Electrified graphene interfaces provide promising paradigm systems for comprehending both short- and long-range neighboring aqueous system impacts.

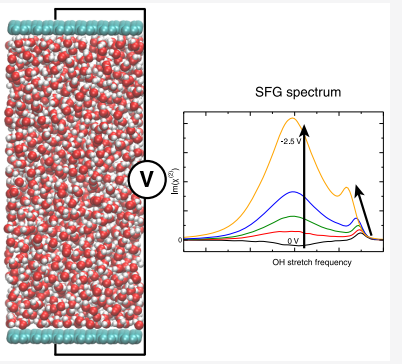

The first layer (or layers) of water molecules at the interface with an electrified material plays a central role in a broad range of processes of fundamental and applied interest, including electrochemical reactivity,[1] electrocatalysis, corrosion, and water desalination.[2] Accordingly, a detailed molecular characterization of an electrified interface's impact on the structure and dynamics of this water layer is of considerable interest. The graphene/water interface is a particularly attractive paradigm system in this connection due to the great practical relevance of carbon/water interfaces[2] and several appealing features of graphene: graphene exhibits a well-defined atomically flat surface,[3] it can be electrified due to its semimetallic character,[4] and it is transparent in the relevant infrared frequency range, making the buried water/graphene interface accessible to surface-specific vibrational spectroscopy experiments.[5] Here we show how molecular dynamics (MD) simulations and sum-frequency generation (SFG) spectra calculations reveal the dramatic effects of applied electric potentials on the structural and dynamical properties of interfacial water layers. In the following, we first describe our simulation methodology, then analyze how the electrode potential changes the structure and the dynamics of the interfacial layers, and finally show how the electrode impacts on water can be probed with SFG spectroscopy.

Our system comprises a slab of 1158 SPC/E water molecules between two rigid single graphene sheets, each containing 240 carbon atoms. The SPC/E potential was shown to provide an excellent description of water dynamics at ambient conditions.[6] In typical SFG experiments,[7] graphene is deposited on a solid substrate and can thus be approximated as immobile. The simulation box is periodically replicated in the two directions parallel to the graphene sheets. Carbon/water nonbonding interactions are described by a Lennard-Jones potential, whose parameters were optimized in ref 8, to reproduce the results of DFT-based MD simulations; such an MD approach allows the necessary extensive and time-extended simulations. Long-range Coulomb interactions are described with a particle-mesh Ewald approach, adapted to the slab geometry. Simulations are run at a series of electrode potentials ranging from 0 to ±2.5 V (potentials of at least ±1.5 V are experimentally accessible,[9] and the largest ±2.5 V potentials are used here to highlight the trends). Graphene carbon atom charges are determined using the constant potential method,[10,11] in which each carbon atom bears a Gaussian charge of inverse width 1.979 $Å^{-1}$, with the charge amplitude determined at each time step such that the potential on each electrode is held fixed; this method has already been successfully employed to describe a broad range of electrified interfaces.[10−14] Each trajectory is first equilibrated in the presence of a 298 K thermostat and subsequently propagated for 4 ns in the microcanonical ensemble using the LAMMPS software,[15] where the constant potential method was implemented.[14] In what follows, all reported error bars provide the 95% confidence intervals determined from block calculations on independent 400 ps (respectively 50 ps)

Received: October 3, 2019
Accepted: January 3, 2020
Published: January 3, 2020

https://dx.doi.org/10.1021/acs.jpclett.9b02924
J. Phys. Chem. Lett. 2020, 11, 624−631

intervals for the structural and dynamical properties (respectively SFG spectra).

We first characterize the effects of increasing electrode potentials on the liquid water structure. These results—which prove to be quite valuable for comprehending the water dynamics and SFG spectra—show that liquid translational and orientational responses at the positive and negative electrodes are in stark contrast. Figure 1a reports the changes in the density profile across the cell (see also Figure S1 for the O and H atom contributions). We first note that at both interfaces the presence of an electrode at 0 V potential does not noticeably affect the water density profile beyond the first two layers (i.e., ∼7 Å from the electrode). However, as soon as a potential difference is applied between the two graphene sheets, the hydration layer densities change in a very different fashion at the two interfaces. At the positive electrode, a growing potential leads predominantly to a more pronounced structuring of the first two layers, with higher and sharper first two density maxima and a lower first density minimum and with a slight shift of the first density maximum toward the graphene sheet. In contrast, at the negative electrode, a more complex restructuring of the first layer occurs, with a progressive splitting of the first layer.

We now embark on an explanation of these observations, first focusing on the water molecule orientations within the first layer, whose boundary is here defined by the first minimum in the density profile. We start with the reference situation at 0 V potential (which is approximately the point of zero charge due to the graphene's apolar nature). Figure 1b (black line) shows the probability distribution of the angle θ between the OH groups of water molecules within the first layer and the vector normal to the graphene sheet pointing toward graphene. Because the average charge on each carbon atom is ≈0, the graphene sheets behave as extended apolar, hydrophobic interfaces. Interfacial water molecules thus tend to form hydrogen bonds with neighboring water molecules, while the flat-interface-imposed geometric constraints force the water hydrogen-bond network to sacrifice some hydrogen bonds, leading to a small fraction of dangling OH groups pointing toward the interface.[16] In contrast to the angular distribution that would be expected in the isotropic, uniform case (dashes), the distribution shows that most water OH groups lie almost tangent to the interface ($\theta \simeq 80°$; see the inset in Figure 1b); another population is oriented away from graphene toward the bulk to form hydrogen bonds with second-layer water molecules ($\theta > 140°$; see the inset in Figure 1b), and finally a small fraction of OH groups are in a "dangling" situation, oriented toward the interface ($\theta < 40°$; see the inset in Figure 1b). This interfacial water molecular arrangement is very similar to that found, e.g., at the air/water interface and at extended hydrophobic interfaces[17,18] (see the SI); it is also consistent with prior simulation results obtained with both classical and DFT-based MD[8,19−21] of water at an uncharged graphene interface.

We now inquire as to the rearrangements induced by applying electrode potentials, starting with negative potentials. Figure 1b shows that the growing negative charge on the carbon atoms favors OH group orientations toward the interface (i.e., dangling OH), with a concomitant depletion in the populations of both OH groups tangent to the interface and those pointing toward bulk water. The splitting of the density profile's first peak in Figure 1a thus arises from the appearance of a new population of water molecules attractively

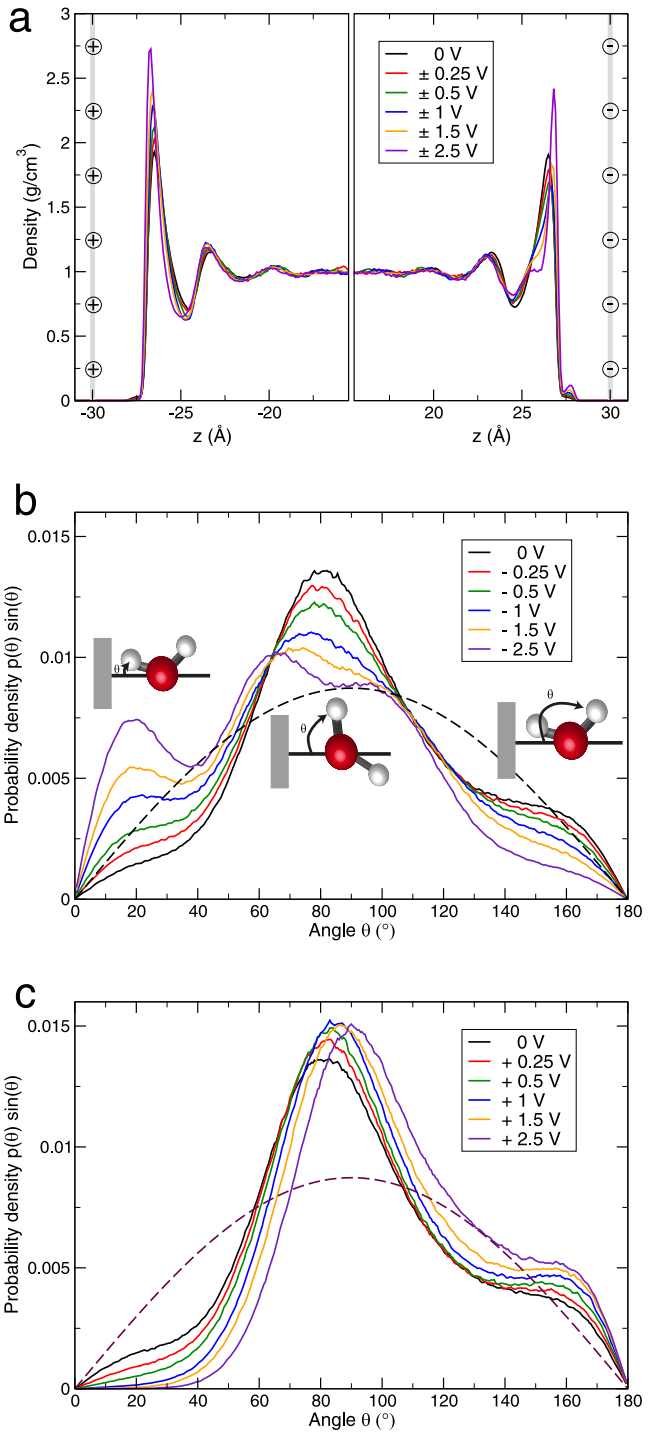

Figure 1. Interfacial water structural properties. (a) Water density profile along the z axis, with the positive interface at $z = -30$ Å and the negative interface at $z = +30$ Å. (b) Angular probability density of water OH groups within the first layer at the negative interface and (c) that at the positive interface. In each case, θ is defined as the angle between the OH group and the vector normal to the interface and pointing toward graphene (see insets in panel b). The dashed lines show the isotropic probability situation.

interacting with the negatively charged graphene via one of their OH groups, in a fashion similar to a donated hydrogen bond. This population is therefore closer to the graphene surface, while the other water molecules within the first layer

https://dx.doi.org/10.1021/acs.jpclett.9b02924
J. Phys. Chem. Lett. 2020, 11, 624−631

do not form such a hydrogen bond and are thus slightly farther from that surface (see Figure S1).

The situation is quite different at the positive electrode interface: Figure 1c shows that increasing potentials only induce minor changes in the water molecule orientations. While the most favorable OH orientation remains that tangent to the interface, the main change induced by the positive electrode potential is the disfavored OH groups' orientations toward the interface caused by the growing carbon positive charges.

This structural analysis has emphasized the strong asymmetry in the water response in the presence of positive and negative electrode potentials. It is important to note that such a result cannot be understood via a simplified point dipole representation of water molecules. However, this inadequacy is not surprising because for first-layer water molecules the molecular size and especially the distance between the oxygen and hydrogen charges cannot be assumed to be much shorter than the water−electrode distance. Indeed, such asymmetry is also found, e.g., in the hydration structures of cations and anions and in the hydration free energies of cations and anions of similar sizes.[22] In contrast, this asymmetry is well-described with the distributed point charge water model used in classical MD.

We now turn to the study of the reorientational and translational dynamics for the water molecules within the first layer at the graphene interface. Our first focus is on the OH group reorientation time correlation function[23] (tcf) relevant for ultrafast infrared anisotropy and NMR measurements[23]

$$C_2^{OH}(t) = \langle P_2[\mathbf{u}_{OH}(0)\cdot\mathbf{u}_{OH}(t)]\rangle \quad (1)$$

where $\mathbf{u}_{OH}(t)$ is the unit vector along an OH group's direction, P_2 is the second-order Legendre polynomial, and the $\langle\cdots\rangle$ ensemble average is performed over all water OH groups within the first layer at $t = 0$. The reorientation time τ_2^{OH} is the long-time decay time of this reorientation tcf.[23] Our results in Figure 2a show that the impact of an electrified interface on water reorientational dynamics differs dramatically for positively and negatively charged electrodes. While water reorientation is markedly slowed by an increasing positive electrode potential, it exhibits a surprising acceleration next to negatively charged electrodes. We further find that, in contrast to the monotonic reorientation slowdown for increasing positive potentials, for negative potentials, τ_2^{OH} exhibits an initial acceleration of the reorientation, followed by an extremum in the neighborhood of −1.5 V, where τ_2^{OH} is smallest and close to the bulk water value; more negative electrode potentials then lead to reorientational slowdown (our key point here is the existence—not the precise location—of this extremum, supported by the clear non-monotonic change in τ_2^{OH} between 0 and −2.5 V).

Water translational dynamics at the interface exhibits the same type of opposite responses to positive and negative electrode potentials just described for reorientation (Figure 2b). It is seen that translational diffusion at the interface is accelerated by negative electrode potentials but slowed by positive potentials. Examination of the components of the displacement parallel and perpendicular to the graphene sheet (Figure 2b) reveals both to be affected in a qualitatively similar fashion. Finally, an analogue of the extremum in the reorientational dynamics at approximately −1.5 V can be found for the translational dynamics orthogonal to the interface but not for that along the plane.

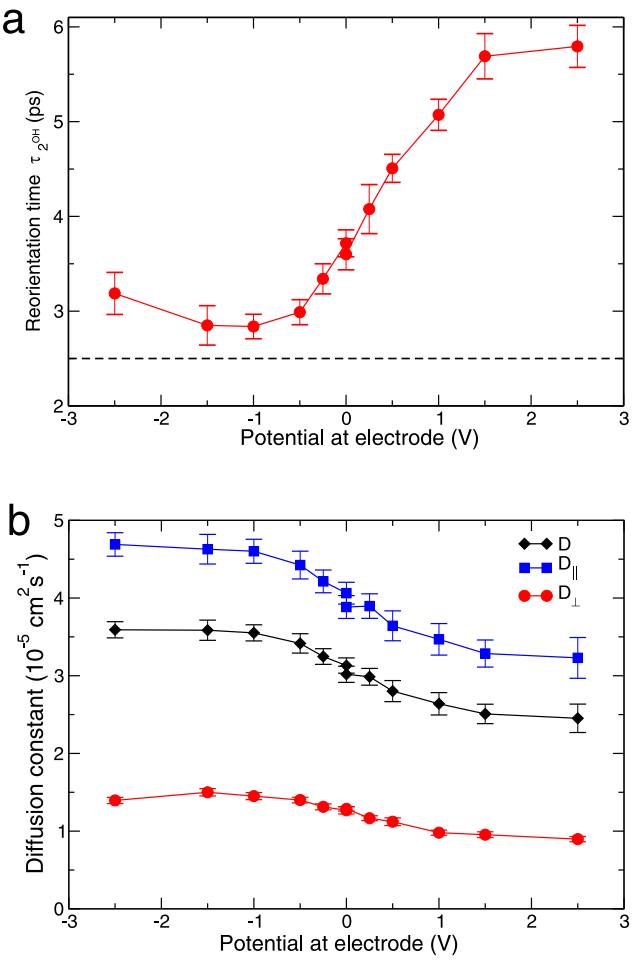

Figure 2. Interfacial water dynamical properties. (a) Reorientation time τ_2^{OH} (eq 1) for water OH groups initially within the interfacial layer at a series of electrode potentials, determined from an exponential fit of C_2^{OH} (eq 1) on the 2−10 ps time interval. (b) Translational diffusion constant of interfacial water molecules, together with its components parallel and perpendicular to the interface, determined from the mean-square displacement of water molecules initially in the first layer via a linear fit over the 2−10 ps interval.

Some of us established[24] that sudden, large-amplitude angular jumps between hydrogen-bond acceptors are the main reorientation pathway for water molecules. These jumps are also intimately connected to the translational dynamics because translational displacements beyond the water molecule's initial solvent cage require hydrogen-bond exchanges. The extended jump model and its subsequent developments have been shown to provide an insightful and almost quantitative description of the impact of a wide variety of different local environments on the hydrogen-bond jump dynamics and thus on the water reorientation time.[23]

As we now argue for water at electrified interfaces, the jump picture again provides an intuitive and molecular understanding of the surprisingly different behaviors at positive and negative electrodes. The key difference is that positive interfaces act as H-bond donors, while negative interfaces act as H-bond acceptors, resulting in different effects on the H-bond jumps.[25] At positive electrodes, our results in Figures 1a,c show that increasing electrode potentials do not qualitatively change the water molecules' arrangement (i.e., the locations of

https://dx.doi.org/10.1021/acs.jpclett.9b02924
J. Phys. Chem. Lett. 2020, 11, 624−631

the density extrema) but produce a more pronounced structuring (i.e., a change in the extrema amplitudes). Prior work by some of us established[26] that such structural enhancements—including, e.g., higher first maximum and lower first minimum in the water−water radial distribution function—hinder the rearrangements necessary for the hydrogen-bond jumps and that these can be quantitatively related to a slowing down of the jump dynamics and thus of the reorientation dynamics.

As for the negative electrode case, the nonmonotonic change in the reorientation dynamics with growing negative charges on the graphene interface seen in Figure 2a is very similar to that observed[27] for the dynamics of water next to a silica surface whose hydrophilicity was changed by progressively switching the surface's atomic charges from a hydrophobic limit of zero up to their full values. The reorientation time's nonmonotonic behavior was shown[27] to be due to a combination of two effects: a change in the populations of OH groups pointing toward the interface and tangentially to the interface and the slowing down in the jump dynamics of OH groups directed toward the interface when the surface charges are increased, strengthening the water/interface attractive interaction. We anticipate the same underlying mechanism to be responsible for the negative electrode potential's effect on the interfacial dynamics of water. Starting from 0 V, decreasing the electrode potential increases the fraction of OH groups pointing toward graphene, and at low potential, the water/graphene interaction remains weak, so that these dangling OH groups reorient rapidly; the average water reorientation time thus decreases. When the electrode potential is very negative, the graphene/water interaction is stronger; the jump time accordingly increases, thus slowing down the average reorientation dynamics and explaining the extremum at intermediate negative potentials. The change in interfacial water dynamics here would originate from the interface's impact on the hydrogen-bond jumps, just as was previously found for a broad range of interfaces.[27,28]

We now examine whether the interfacial water layer's structural rearrangements resulting from different electrode potentials that we have described can be probed experimentally. Vibrational SFG suggests itself as a tool because it has been successfully used to characterize water molecules at a range of aqueous interfaces, including air/water, alkane/water, and silica/water interfaces.[29−31] The buried interface between an aqueous solution and an electrochemical material presents a considerable challenge,[32−34] but graphene is a promising system here because it combines an atomically well-defined surface[3] and IR transparency in the OH stretch region.[5] Recent experimental results are encouraging: SFG spectra at an uncharged graphene/water interface have been measured,[5] and a successful implementation in an electrochemical cell has been reported,[7] although experimental challenges to prevent water intercalation between the substrate and graphene remain.

We pursue SFG's applicability here by calculating the resonant susceptibility accessible in SFG measurements with heterodyne detection[30,31,35]

$$\chi^{(2)}_{pqr}(\omega) = \frac{i\omega}{k_B T}\int_0^\infty dt\, e^{i\omega t}\langle \alpha_{pq}(t)\mu_r(0)\rangle \qquad (2)$$

where α is the water polarizability tensor, μ is the dipole moment, and the pqr indices designate the tensor elements in the xyz space-fixed coordinate frame. In what follows, we focus on the ssp polarization scheme, i.e., $pqr = yyz$, because its interpretation is the most straightforward. The water molecular polarizability and dipole are determined at every step of the simulation using the empirical map developed in ref 36, connecting these quantities to the local electric field experienced by the water H atom along the OH axis. This method was successfully applied to the air/water SFG spectra.[36] We follow the same approach to calculate the spectrum that would be measured using a dilute HOD in liquid D_2O solution; this isotopic mixture allows probing of a local OH mode, decoupled from the other OD stretches in the liquid, including the same water molecule's OD group. In order to separately determine the SFG spectra at each of the system's two interfaces, we use a switching function centered on the simulation box's middle and based on the oxygen atom position, following recent suggestions.[37,38]

The resulting SFG spectrum for water at the graphene interface at 0 V (Figure 3a) is generally typical of those already found at air/water interfaces.[30,31,35,36,38] It exhibits two main bands, a high-frequency ≃3700 cm^{-1} positive band and a lower-frequency ≃3400 cm^{-1} negative band. The positive band arises from OH groups that are pointing toward the interface with graphene, and its high frequency implies that these OH

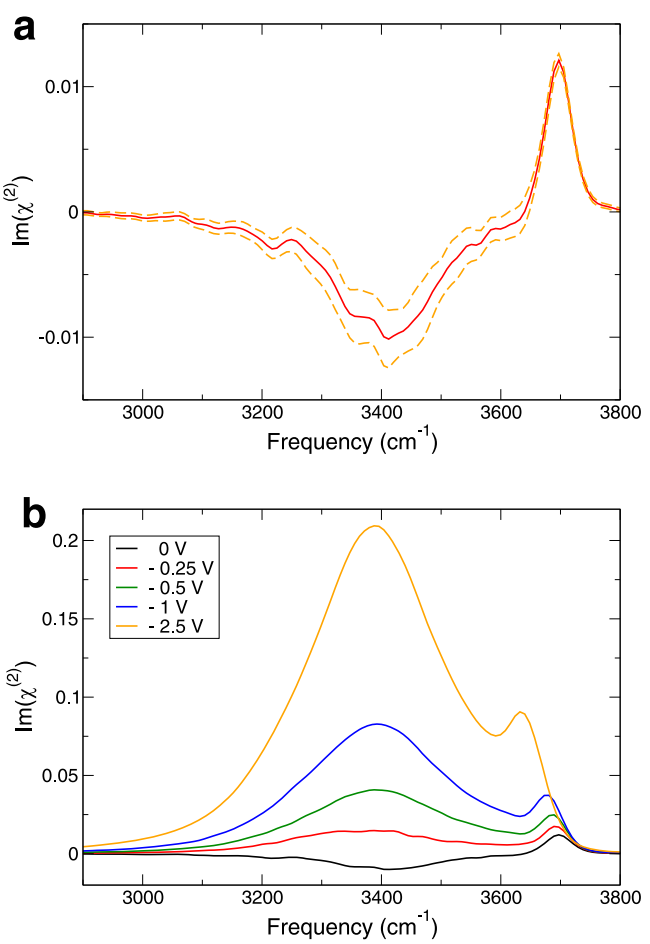

Figure 3. Calculated phase-resolved vibrational SFG spectra of water (after convolution with a 10 cm^{-1} Gaussian) (a) at 0 V with the average spectrum (red) and the 95% confidence interval (orange dashes), (b) at the negatively charged graphene interfaces for a series of applied potentials (the calculated 3400 cm^{-1} peak height is underestimated due to the cutoff applied to the $\chi^{(3)}$ contribution beyond half of the simulation box length).

https://dx.doi.org/10.1021/acs.jpclett.9b02924
J. Phys. Chem. Lett. 2020, 11, 624−631

groups are weakly or not hydrogen-bonded. (At the air/water interface, this band was shown to arise from "dangling" OH groups at the surface.[16]) Regarding the lower-frequency band, its sign implies that it originates from water OH groups pointing away from the interface, toward the bulk liquid, and its average frequency shows that these OH groups are engaged in hydrogen bonds. The calculated 0 V SFG spectrum is thus consistent with the angular distribution shown in Figure 1b, but it is mostly sensitive to OH groups pointing toward and away from the graphene/water interface; the dominant tangent OH group population does not lead to a SFG signal for the chosen ssp polarization.

Our present spectrum is in excellent agreement with that recently obtained by DFT-based MD simulations at a graphene interface with no applied potential[39] (the OD stretch vibration was probed in the latter, resulting in a red-shifted spectrum). Some first experimental measurements addressing the water SFG spectrum at the graphene interface have recently been reported.[5] The overall SFG intensity was measured; in the absence of phase information, the sign of $\chi^{(2)}$ is thus not known. The measured spectrum does exhibit low- and high-frequency bands, as in Figure 3a, although the dangling OH band's intensity seems to be quite a bit smaller than that in both of our calculations and those of ref 39. However, the experimental setup does not use the isotopic mixture studied in our simulations and in addition employs a graphene sheet on a polar aluminum oxide (sapphire) support layer, whose electrostatic interactions with water might be responsible for the observed difference.

We now consider how vibrational SFG spectroscopy can probe the structural rearrangement within the interfacial layer that is induced by an electrode potential. Here we focus on the negatively charged interface, where the rearrangement is more pronounced. The SFG spectra shown in Figure 3b exhibit a dramatic change with increasingly negative potentials.

The first important change is the simultaneous growth and red shift of the high-frequency, dangling OH band. Both are due to the growing negative charges on the carbon atoms. The latter stabilize OH groups oriented toward the interface (as visible in Figure 1b), thus increasing their population and the band amplitude; further, the strengthening of the OH−graphene interaction red shifts the OH vibrational frequency, as found for a stronger hydrogen-bond acceptor.

The second major SFG spectra change in Figure 3b is the spectacular growth of the ≃3400 cm^{-1} hydrogen-bonded band. This band is negative at 0 V and becomes positive for increasingly negative electrode potentials, growing to such extent that it greatly surpasses the amplitude of the dangling OH band for the most negative potentials investigated. However, while the band's amplitude dramatically changes with the electrode potential, its central frequency remains unchanged. At negative potentials, the positive sign of $\mathrm{Im}[\chi^{(2)}]$ implies that the OH groups causing the signal are pointing toward graphene, while at the same time the essentially constant ≃3400 cm^{-1} frequency shows that these groups are donating strong hydrogen bonds. These two features imply that these OH groups cannot be in the first layer next to the graphene interface. The question then is, where are they located?

This query brings us to a long-standing question in SFG spectroscopy: what is the depth of the interface that is experimentally probed?[40] Because SFG specifically probes water molecules residing in a noncentrosymmetric environment, answering this question amounts to determining how far the interface-induced perturbation extends. In the case of the air/water interface, it was established that only the two topmost layers contribute to the SFG spectrum,[41] but it was shown that for, e.g., surfactant/water interfaces the probed depth changes with vibrational frequency and can have a greater extent.[42] Accordingly, when different electrode potentials are applied, we undertook direct calculation of the SFG spectrum's contributions from the successive water layers.

We first consider the 0 V spectrum as an essential reference. Figure 4a shows the depth-dependent spectrum along the distance z_H from the water OH group hydrogen atom to the graphene plane. This figure allows us to considerably refine and deepen the molecular interpretation of the SFG spectrum in Figure 3a. First, it confirms that the high-frequency ≃3700 cm^{-1} peak indeed comes almost exclusively from first-layer OH groups pointing toward the interface, as shown by the short z_H ≃ 2.7 Å distance where this peak appears. Second, and in contrast, the $\chi^{(2)}$ signal at lower frequencies includes contributions not only from the first layer but also from the second layer. This latter region requires a more detailed discussion, which we initiate with Figure 4a, which shows an alternation of positive and negative contributions for growing z_H due to the two OH groups carried by the water molecules in each layer. Here it is useful to recall that the density profile maxima in Figure 1a provide the water oxygen atoms' positions in each layer, and the first two peaks are successively located at 3.5 and 6.7 Å from the interface at 0 V. We can then see that

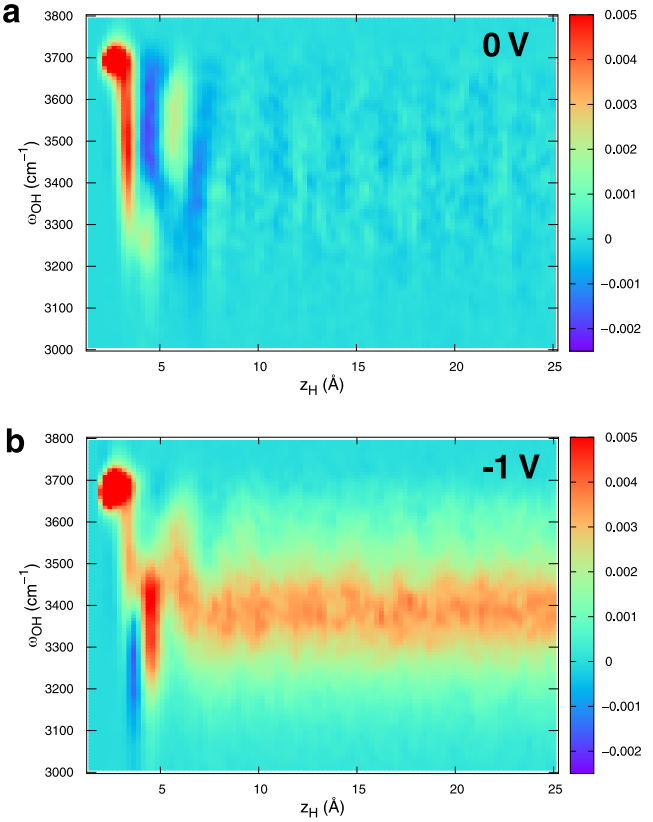

Figure 4. Depth-dependent contributions to the SFG spectrum along the distance z_H between the water hydrogen atom and the graphene interface at (a) 0 and (b) −1 V. At each distance, the eq 2 $\chi^{(2)}_{pqr}(\omega)$ calculation is restricted to water OH groups with a specific z_H value at t = 0.

https://dx.doi.org/10.1021/acs.jpclett.9b02924
J. Phys. Chem. Lett. 2020, 11, 624−631

the negative band at ≃3400 cm^{-1} results from a series of contributions—two for each layer—with an important cancellation of effects. For the first-layer contributions, there is (i) a positive one at $z_H \simeq 3.3$ Å arising from OH groups having undergone a large-amplitude librational motion, which brings them from their tangent equilibrium hydrogen-bonded arrangement into configurations pointing toward the surface, and (ii) a negative one from OH groups pointing toward the bulk ($z_H \simeq 4.3$ Å); this is the dominant term in the spectrum's negative band. (We pause to note that contribution (ii) is centered at a higher frequency than in the resulting SFG spectrum (3500 vs 3400 cm^{-1}) and that the apparent frequency shift results from a more pronounced cancellation with term (i) at higher frequency.) For the second layer contributions, there is (iii) a positive one from OH groups pointing toward the interface ($z_H \simeq 5.7$ Å) and finally (iv) a negative one from OH groups pointing away from the interface ($z_H \simeq 7.0$ Å). No significant SFG contribution was found beyond the second layer at 0 V.

We now contrast these zero potential results with the situation at −1 V, shown in Figure 4b. First, the enhancement and red shift of the high-frequency peak are now very clear, and it remains exclusively due to first-layer OH groups pointing toward the interface. However, the lower-frequency part of the spectrum changes dramatically with respect to the 0 V case. First, the first two layers' contributions are now strongly affected; as shown in Figure 1b's structural analysis, the number of OH groups pointing toward the bulk decreases, thus decreasing their negative SFG spectrum contribution, while most interfacial OH groups remain approximately tangent to the graphene electrode and bring a small signal with the ssp polarization. However, the most important change is the presence of contributions not only from the closest two water layers but also from water molecules much deeper than those layers. We see that the contribution to the SFG spectrum continues past them, becoming approximately constant for distances greater than ≃7 Å. This long-range signal arises from the static electric field created between the graphene sheets and induces a so-called $\chi^{(3)}$ signal.

The importance of the $\chi^{(3)}$ contribution at charged interfaces has already been recognized and abundantly discussed in the literature (see, e.g., refs 31, 40, and 43−49). However, in most studied systems so far—including, e.g., charged silica/water and lipid/water interfaces—the surface charges are changed by modifying the pH or increasing the concentration in ions[40] or charged surfactants,[48,49] all of which induce a modification in the interface chemistry. The present electrified graphene/water interface thus offers an interesting platform to study long-range $\chi^{(3)}$ effects because the surface charge can be independently set by changing the applied electrode potential. Ongoing work is being devoted to analysis of this contribution.

Our study has two key features. First, it has revealed that an electrode electric potential has a profound impact on the water layer in contact with a graphene sheet. The algebraic sign of the applied potential is found to have opposite effects on the interfacial water dynamics: while a positive potential slows down the reorientational and translational dynamics of water, a negative potential accelerates the interfacial water dynamics. The general features of these dynamics can be comprehended via the jump picture for water hydrogen-bond exchange; this aspect will be pursued in detail elsewhere. The second key feature concerns vibrational SFG spectroscopic applicability at the interface. We show that the arrangement of water molecules at the graphene interface at 0 V is very similar to that found at the air/water interface and that SFG spectroscopy can specifically probe this interface. However, when nonvanishing electrode potentials are applied, the resulting static electric field induces a long-range response, which makes the SFG spectra interpretation a greater challenge, one that we will address in the future.

■ ASSOCIATED CONTENT

Supporting Information

The Supporting Information is available free of charge at https://pubs.acs.org/doi/10.1021/acs.jpclett.9b02924.

Details of system preparation, density profiles, and SFG spectra calculations (PDF)

■ AUTHOR INFORMATION

Corresponding Author

Damien Laage − *École normale Supérieure, PSL University, Sorbonne Université, CNRS, Paris, France;* orcid.org/0000-0001-5706-9939; Email: damien.laage@ens.fr

Other Authors

Yiwei Zhang − *École normale Supérieure, PSL University, Sorbonne Université, CNRS, Paris, France*

Hilton B. de Aguiar − *École normale supérieure, PSL University, CNRS, Paris, France;* orcid.org/0000-0002-2426-0371

James T. Hynes − *École normale Supérieure, PSL University, Sorbonne Université, CNRS, Paris, France, and University of Colorado, Boulder, Colorado;* orcid.org/0000-0003-2683-0304

Complete contact information is available at: https://pubs.acs.org/10.1021/acs.jpclett.9b02924

Notes

The authors declare no competing financial interest.

■ ACKNOWLEDGMENTS

This work was partly supported by LabEX ENS-ICFP: ANR-10-LABX-0010/ANR- 10-IDEX-0001-02 PSL* (HBdA) and NSF Grant CHE-1112564 (J.T.H.).

■ REFERENCES

(1) Ambrosi, A.; Chua, C.; Bonanni, A.; Pumera, M. Electrochemistry of graphene and related materials. *Chem. Rev.* **2014**, *114*, 7150−7188.

(2) Striolo, A.; Michaelides, A.; Joly, L. The Carbon-Water Interface: Modeling Challenges and Opportunities for the Water-Energy Nexus. *Annu. Rev. Chem. Biomol. Eng.* **2016**, *7*, 533−556.

(3) Lui, C.; Liu, L.; Mak, K.; Flynn, G.; Heinz, T. Ultraflat graphene. *Nature* **2009**, *462*, 339−341.

(4) Eda, G.; Mattevi, C.; Yamaguchi, H.; Kim, H.; Chhowalla, M. Insulator to Semimetal Transition in Graphene Oxide. *J. Phys. Chem. C* **2009**, *113*, 15768−15771.

(5) Singla, S.; Anim-Danso, E.; Islam, A. E.; Ngo, Y.; Kim, S. S.; Naik, R. R.; Dhinojwala, A. Insight on Structure of Water and Ice Next to Graphene Using Surface-Sensitive Spectroscopy. *ACS Nano* **2017**, *11*, 4899−4906.

(6) Schmidt, J.; Roberts, S.; Loparo, J.; Tokmakoff, A.; Fayer, M.; Skinner, J. Are water simulation models consistent with steady-state

and ultrafast vibrational spectroscopy experiments? *Chem. Phys.* **2007**, *341*, 143−157.
(7) Dreier, L. B.; Liu, Z.; Narita, A.; van Zadel, M.-J.; Müllen, K.; Tielrooij, K.-J.; Backus, E. H. G.; Bonn, M. Surface-Specific Spectroscopy of Water at a Potentiostatically Controlled Supported Graphene Monolayer. *J. Phys. Chem. C* **2019**, *123*, 24031.
(8) Rana, M.; Chandra, A. Ab initio and classical molecular dynamics studies of the structural and dynamical behavior of water near a hydrophobic graphene sheet. *J. Chem. Phys.* **2013**, *138*, 204702.
(9) Bie, Y.; Horng, J.; Shi, Z.; Ju, L.; Zhou, Q.; Zettl, A.; Yu, D.; Wang, F. Vibrational spectroscopy at electrolyte/electrode interfaces with graphene gratings. *Nat. Commun.* **2015**, *6*, 7593.
(10) Siepmann, J. I.; Sprik, M. Influence of surface topology and electrostatic potential on water/electrode systems. *J. Chem. Phys.* **1995**, *102*, 511.
(11) Reed, S.; Lanning, O.; Madden, P. Electrochemical interface between an ionic liquid and a model metallic electrode. *J. Chem. Phys.* **2007**, *126*, 084704.
(12) Willard, A. P.; Reed, S. K.; Madden, P. A.; Chandler, D. Water at an electrochemical interface—a simulation study. *Faraday Discuss.* **2009**, *141*, 423−441.
(13) Merlet, C.; Péan, C.; Rotenberg, B.; Madden, P.; Simon, P.; Salanne, M. Simulating Supercapacitors: Can We Model Electrodes As Constant Charge Surfaces. *J. Phys. Chem. Lett.* **2013**, *4*, 264−268.
(14) Wang, Z.; Yang, Y.; Olmsted, D.; Asta, M.; Laird, B. Evaluation of the constant potential method in simulating electric double-layer capacitors. *J. Chem. Phys.* **2014**, *141*, 184102.
(15) Plimpton, S. Fast parallel algorithms for short-range molecular dynamics. *J. Comput. Phys.* **1995**, *117*, 1−19.
(16) Du, Q.; Freysz, E.; Shen, Y. R. Surface vibrational spectroscopic studies of hydrogen bonding and hydrophobicity. *Science* **1994**, *264*, 826−828.
(17) Stirnemann, G.; Rossky, P. J.; Hynes, J. T.; Laage, D. Water Reorientation, Hydrogen-Bond Dynamics and 2D-IR Spectroscopy next to an Extended Hydrophobic Surface. *Faraday Discuss.* **2010**, *146*, 263−281.
(18) Xiao, S.; Figge, F.; Stirnemann, G.; Laage, D.; McGuire, J. A. Orientational Dynamics of Water at an Extended Hydrophobic Interface. *J. Am. Chem. Soc.* **2016**, *138*, 5551−5560.
(19) Ho, T. A.; Striolo, A. Molecular dynamics simulation of the graphene-water interface: comparing water models. *Mol. Simul.* **2014**, *40*, 1190−1200.
(20) Ruiz-Barragan, S.; Muñoz-Santiburcio, D.; Marx, D. Nano-confined Water within Graphene Slit Pores Adopts Distinct Confinement-Dependent Regimes. *J. Phys. Chem. Lett.* **2019**, *10*, 329−334.
(21) Subasinghege Don, V.; David, R.; Du, P.; Milet, A.; Kumar, R. Interfacial Water at Graphene Oxide Surface: Ordered or Disordered. *J. Phys. Chem. B* **2019**, *123*, 1636−1649.
(22) Rajamani, S.; Ghosh, T.; Garde, S. Size dependent ion hydration, its asymmetry, and convergence to macroscopic behavior. *J. Chem. Phys.* **2004**, *120*, 4457−4466.
(23) Laage, D.; Stirnemann, G.; Sterpone, F.; Rey, R.; Hynes, J. T. Reorientation and Allied Dynamics in Water and Aqueous Solutions. *Annu. Rev. Phys. Chem.* **2011**, *62*, 395−416.
(24) Laage, D.; Hynes, J. T. A molecular jump mechanism of water reorientation. *Science* **2006**, *311*, 832−835.
(25) Fogarty, A. C.; Duboué-Dijon, E.; Sterpone, F.; Hynes, J. T.; Laage, D. Biomolecular hydration dynamics: a jump model perspective. *Chem. Soc. Rev.* **2013**, *42*, 5672−5683.
(26) Wilkins, D. M.; Manolopoulos, D. E.; Pipolo, S.; Laage, D.; Hynes, J. T. Nuclear Quantum Effects in Water Reorientation and Hydrogen-Bond Dynamics. *J. Phys. Chem. Lett.* **2017**, *8*, 2602−2607.
(27) Stirnemann, G.; Castrillón, S.; Hynes, J. T.; Rossky, P.; Debenedetti, P.; Laage, D. Non-monotonic dependence of water reorientation dynamics on surface hydrophilicity: competing effects of the hydration structure and hydrogen-bond strength. *Phys. Chem. Chem. Phys.* **2011**, *13*, 19911−19917.
(28) Laage, D.; Elsaesser, T.; Hynes, J. T. Water Dynamics in the Hydration Shells of Biomolecules. *Chem. Rev.* **2017**, *117*, 10694−10725.
(29) Shen, Y. R.; Ostroverkhov, V. Sum-frequency vibrational spectroscopy on water interfaces: polar orientation of water molecules at interfaces. *Chem. Rev.* **2006**, *106*, 1140−1154.
(30) Ishiyama, T.; Imamura, T.; Morita, A. Theoretical Studies of Structures and Vibrational Sum Frequency Generation Spectra at Aqueous Interfaces. *Chem. Rev.* **2014**, *114*, 8447−8470.
(31) Nihonyanagi, S.; Yamaguchi, S.; Tahara, T. Ultrafast Dynamics at Water Interfaces Studied by Vibrational Sum Frequency Generation Spectroscopy. *Chem. Rev.* **2017**, *117*, 10665−10693.
(32) Zheng, W.; Tadjeddine, A. Adsorption processes and structure of water molecules on Pt(110) electrodes in perchloric solutions. *J. Chem. Phys.* **2003**, *119*, 13096−13099.
(33) Nihonyanagi, S.; Ye, S.; Uosaki, K.; Dreesen, L.; Humbert, C.; Thiry, P.; Peremans, A. Potential-dependent structure of the interfacial water on the gold electrode. *Surf. Sci.* **2004**, *573*, 11−16.
(34) Schultz, Z. D.; Shaw, S. K.; Gewirth, A. A. Potential Dependent Organization of Water at the Electrified Metal-Liquid Interface. *J. Am. Chem. Soc.* **2005**, *127*, 15916−15922.
(35) Morita, A.; Hynes, J. T. A Theoretical Analysis of the Sum Frequency Generation Spectrum of the Water Surface. II. Time-Dependent Approach. *J. Phys. Chem. B* **2002**, *106*, 673−685.
(36) Auer, B.; Skinner, J. Vibrational sum-frequency spectroscopy of the liquid/vapor interface for dilute HOD in D(2)O. *J. Chem. Phys.* **2008**, *129*, 214705.
(37) Byrnes, S. J.; Geissler, P. L.; Shen, Y. Ambiguities in surface nonlinear spectroscopy calculations. *Chem. Phys. Lett.* **2011**, *516*, 115−124.
(38) Ni, Y.; Skinner, J. Communication: Vibrational sum-frequency spectrum of the air-water interface, revisited. *J. Chem. Phys.* **2016**, *145*, 031103.
(39) Ohto, T.; Tada, H.; Nagata, Y. Structure and dynamics of water at water-graphene and water-hexagonal boron-nitride sheet interfaces revealed by ab initio sum-frequency generation spectroscopy. *Phys. Chem. Chem. Phys.* **2018**, *20*, 12979−12985.
(40) Gonella, G.; Lütgebaucks, C.; de Beer, A. G. F.; Roke, S. Second Harmonic and Sum-Frequency Generation from Aqueous Interfaces Is Modulated by Interference. *J. Phys. Chem. C* **2016**, *120*, 9165−9173.
(41) Morita, A.; Hynes, J. T. A theoretical analysis of the sum frequency generation spectrum of the water surface. *Chem. Phys.* **2000**, *258*, 371−390.
(42) Roy, S.; Gruenbaum, S.; Skinner, J. Theoretical vibrational sum-frequency generation spectroscopy of water near lipid and surfactant monolayer interfaces. *J. Chem. Phys.* **2014**, *141*, 18C502.
(43) Ong, S.; Zhao, X.; Eisenthal, K. B. Polarization of water molecules at a charged interface: second harmonic studies of the silica/water interface. *Chem. Phys. Lett.* **1992**, *191*, 327−335.
(44) de Beer, A. G.; Campen, R. K.; Roke, S. Separating surface structure and surface charge with second-harmonic and sum-frequency scattering. *Phys. Rev. B: Condens. Matter Mater. Phys.* **2010**, *82*, 235431.
(45) Ohno, P.; Wang, H.; Geiger, F. Second-order spectral lineshapes from charged interfaces. *Nat. Commun.* **2017**, *8*, 1032.
(46) Joutsuka, T.; Hirano, T.; Sprik, M.; Morita, A. Effects of third-order susceptibility in sum frequency generation spectra: a molecular dynamics study in liquid water. *Phys. Chem. Chem. Phys.* **2018**, *20*, 3040−3053.
(47) Hore, D. K.; Tyrode, E. Probing Charged Aqueous Interfaces Near Critical Angles: Effect of Varying Coherence Length. *J. Phys. Chem. C* **2019**, *123*, 16911−16920.
(48) Wen, Y.; Zha, S.; Liu, X.; Yang, S.; Guo, P.; Shi, G.; Fang, H.; Shen, Y.; Tian, C. Unveiling Microscopic Structures of Charged Water Interfaces by Surface-Specific Vibrational Spectroscopy. *Phys. Rev. Lett.* **2016**, *116*, 016101.

https://dx.doi.org/10.1021/acs.jpclett.9b02924
J. Phys. Chem. Lett. 2020, 11, 624−631

(49) Dreier, L.; Nagata, Y.; Lutz, H.; Gonella, G.; Hunger, J.; Backus, E.; Bonn, M. Saturation of charge-induced water alignment at model membrane surfaces. *Sci. Adv.* **2018**, *4*, No. eaap7415.

https://dx.doi.org/10.1021/acs.jpclett.9b02924
J. Phys. Chem. Lett. 2020, 11, 624−631